JOURNAL OF THE KOREAN ASTRONOMICAL SOCIETY
27: 31 ~ 44, 1994

DISTRIBUTION AND KINEMATICS OF FORMALDEHYDE IN DARK CLOUDS IN M17 AND NGC 2024*

MINN, Y. K.
Department of Astronomy and Space Science
Kyung Hee University, Suwon 449-701
AND
LEE, Y. B.
Department of Science Education
Seoul National University of Education, Seoul 137-742
(Received Mar. 31, 1994; Accepted Apr. 13, 1994)

ABSTRACT

The 4.8GHz formaldehyde absorption line in the dark clouds in M17 and NGC 2024 regions has been mapped. In both nebulae, we detected two H_2CO line components. In M17, the 24km s^{-1} cloud is closely associated with the HII region located in front of the radio continuum source, and the 19km s^{-1} cloud is associated with the visual dark clouds with a larger extent which are closer to us. The 19km s^{-1} cloud has a mass motion approaching to the HII region. In both clouds, a velocity gradient from the north-east to the south-west directions is observed. The linewidth has no variation indicating no collapsing motion. In NGC 2024, the 9km s^{-1} feature is extended along the dark bar in front of the bright nebula and a weak second component at 13km s^{-1} is confined to the immediate vicinity of the radio source. Indications are that the 9km s^{-1} cloud is physically associated with the dark bar and the 13km s^{-1} cloud is located behind the radio source. The angular extent, the column density, and the total mass of the clouds are derived. The radial velocities of other molecular lines observed in these clouds are compared.

Key Words : interstellar medium, molecules (H_2CO), molecular clouds (M17, NGC 2024)

I. INTRODUCTION

The HII regions, M17 (Omega nebula, W38, S45, NGC 6618) and NGC 2024 (Orion B, W12) are strong radio sources associated with dense dark clouds. In both nebulae, a heavy-obscuring dark lane which may have obscured a large portion of the bright Hα emission near the central part of the cloud lies across the face of the HII regions. The exciting stars in the region of M17 are heavily obscured with extinction more than 11 magnitudes (Chini *et al.*, 1980) and the radio continuum peak of NGC 2024 is hidden by the dark lane.

There have been detected various molecular lines, molecular maser sources, infrared sources, and cocoon stars, all indicating an active star formation in the regions [see reviews by Goudis (1976)].

Mappings in radio continuum, radio recombination lines, and molecular lines have also been made in the regions of radio continuum peaks. Large scale molecular line surveys around the continuum peak positions have been made for M17 in ^{12}CO, ^{13}CO, and $C^{18}O$ by many authors (Liszt, 1973; Lada *et al.*, 1974; Elmegreen and

* This paper was supported by 1992 Research Fund of Kyung Hee University.

Lada, 1976; Thronson and Lada, 1983; Rainey *et al.*, 1987; Stutzki and Gusten, 1990; Greaves *et al.*, 1992), H_2CO (Lada and Chaisson, 1975; Bieging *et al.*, 1982), and NH_3 (Massi *et al.*, 1988). For NGC 2024, surveys in ^{12}CO (Tucker *et al.*, 1973; Milman *et al.*, 1975; Watt *et al.*, 1979), OH (Goss *et al.*, 1976), H_2CO (Bieging *et al.*, 1982), CS and HCN (Thronson *et al.*, 1984), and NH_3 and CS (Schulz *et al.*, 1991) have been made.

These surveys show that the structure and kinematics of the clouds are complex. The molecular lines have several components at different velocities, and their spatial distributions appear to be extended to a large area with many fragments or clumps in M17 (Lada, 1976; Stutzki and Gusten, 1990) and beyond the radio continuum emission region in NGC 2024 (Watt *et al.*, 1979). There are also found areas of star formation (Rainey *et al.*, 1987; Schulz *et al.*, 1991). There is an intense CO emission peak at about 4′ southwest of the radio continuum center in M17 (M17SW) where a number of other molecules (see Table 1 of this paper) and intense infrared sources were found (Lada *et al.*, 1974; Rainey *et al.*, 1987).

Even though it is generally known that dust is associated with molecules, it is not clear yet how closely the visual dust lane is related to the distribution of the H_2CO molecule in the HII and its surrounding regions.

We report here mapping of dark clouds in the regions surrounding M17 and NGC 2024 in the 4.83GHz H_2CO line with a 6.6 arcmin beam and a half-beam spacing. We examined the structure and kinematics of the H_2CO clouds and compared them with the distribution of the apparent dust clouds. We also compared our results with the kinematics of other molecular lines observed in the regions.

II. OBSERVATIONS

Observations were made with the 43-m telescope of the NRAO[1]. The receiver was the 413-channel autocorrelator equipped with a cooled 6-cm parametric amplifier. At 4.83GHz, the beamwidth of the antenna was 6.6 arcmin and the antenna and the beam efficiencies are ~ 0.5 and ~ 0.8 respectively. A linearly polarized feed with E-plane in the north-south direction was used. The system noise temperature was approximately 60K throughout the observation. The spectral window was 1.25MHz for M17 with an effective frequency resolution of 3.94kHz (0.24km s^{-1}), and 625kHz with a resolution of 1.97kHz (0.12km s^{-1}) for NGC 2024. The H_2CO rest frequency of 4829.65961MHz was used. All velocities refer to the local standard of rest.

We started our mapping from the darkest part of the apparent dark dust lanes to the outer parts where the line intensity falls to undetectable level. The observing points are spaced at one-half of the beamwidth ($=3'$). In addition, we also observed at the peak positions of the radio continuum given by Schraml and Mezger (1969). A total of 31 points in M17 and 30 points in NGC 2024 have been observed. The observed line profiles are Gaussian fitted to derive the velocity and linewidth.

III. FORMALDEHYDE IN M17

1. Intensity Distribution

We detected two H_2CO clouds in the direction of M17; one, an intense feature with narrow linewidths at a velocity of about 24km s^{-1} and the other, a feature with broad linewidths at about 19km s^{-1}. The 24km s^{-1} cloud is confined to the immediate vicinity of the radio continuum region, while the 19km s^{-1} cloud has a much larger spatial extent generally matching the apparent dark lane with its center at the darkest part of the dark cloud. Lada and Chaisson (1975) also observed two H_2CO lines at the same velocities as above in M17. However, Bieging *et al.* (1982) found an additional weak feature at the velocity range from 8 to 14km s^{-1} in the direction of the continuum source.

Contour maps of the antenna temperature of the H_2CO line are presented in Figure 1a for the 24km s^{-1} cloud and in Figure 1b for the 19km s^{-1} cloud. In Figure 1b, the contour lines are superimposed on the Palomar Observatory Sky Survey (POSS) red print.

1) Operated by the Associated Universities, Inc., under contract with the National Science Foundation.

The 24km s^{-1} cloud shows little correlation with the apparent distribution of the dark cloud in the region. It is rather similar in shape to the 6-cm radio emission distribution (Mezger and Henderson, 1967; Altenhoff *et al.*, 1979) and the peak positions of the H_2CO cloud and the radio continuum emission coincide within the uncertainty of the beamwidth. The extent of the molecular cloud is also comparable to that of the radio continuum emission with a brightness temperature of $T_b = 25K$ at 6cm. The brightness temperature ratios of the continuum and the H_2CO line $|T_b$ (continuum)$/T_b$ (H_2CO line)$|$ in the region remain generally constant at ~ 35. The close correlation between the H_2CO line and the radio continuum emission suggests that the 24km s^{-1} feature arises by the absorption of the continuum from the radio source in the background. Therefore, it is clear that this feature is located in front of the radio continuum source. Lada (1976) separated a 23km s^{-1} CO component which coincides with the visible HII region.

The mean optical depth of this cloud is low at $\tau = \sim 0.03$ and the distribution is generally uniform. The equivalent width, $W = \int [1 - e^{-\tau(v)}] dv$ of the H_2CO line, however, increases with a small gradient towards the north with a maximum value of 0.06km s^{-1} at the northern edge and a minimum value of 0.03km s^{-1} at the southern edge of the cloud. It indicates that this cloud would have extended to farther north with a larger dimension than we observed. However, with the small optical depth of the cloud, detection of the line would be impossible against the 2.7K cosmic background radiation, since there presents no continuum radiation from the HII region. If we assume T_{ex} of H_2CO in the cloud is 1.7K and $\tau = 0.03$ and the telescope beam fills the cloud, the line temperature would be 0.03K which is below the noise level of our observations.

The angular size of this cloud is about $14' \times 11'$ in arc which corresponds to $62pc^2$ if we adopt a distance of 2.2kpc (Chini *et al.*, 1980). The mean column density and mass of the 24km s^{-1} formaldehyde cloud are N (H_2CO) $= 8.5 \times 10^{11} cm^{-2}$ and M (H_2CO) $= 3.7 \times 10^{-6} M_\odot$ respectively which are very close to the values given by Lada and Chaisson (1975). If we take N (H_2CO)/N (H_2) $= 4 \times 10^{-9}$ (Minn and Greenberg, 1979) and assume the hydrogen is mostly in the molecular form, the total mass of the cloud is $M_{total} = 330 M_\odot$.

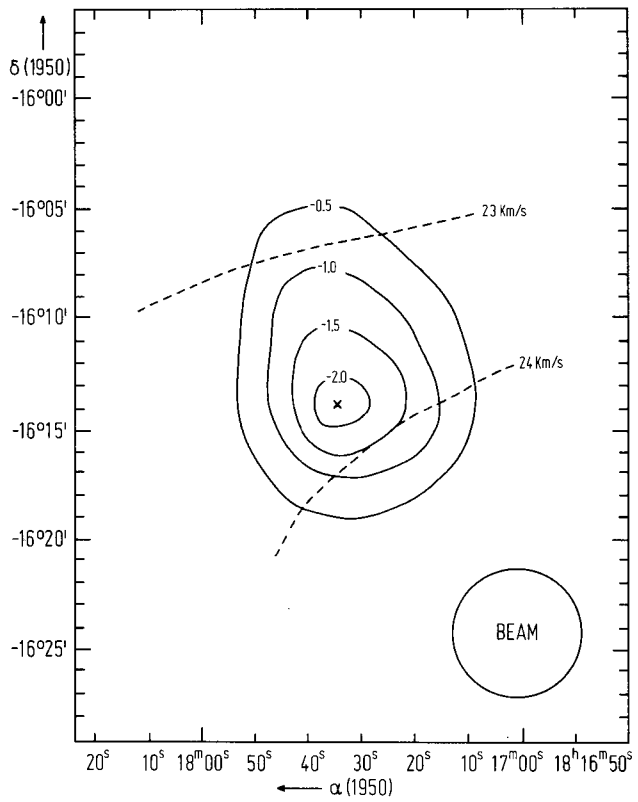

Fig. 1a. Contour map of the antenna temperature (K) of the 24km s^{-1} H_2CO line in M17. The unit of T_A is K. The radial velocities of the lines are shown in dashed lines.

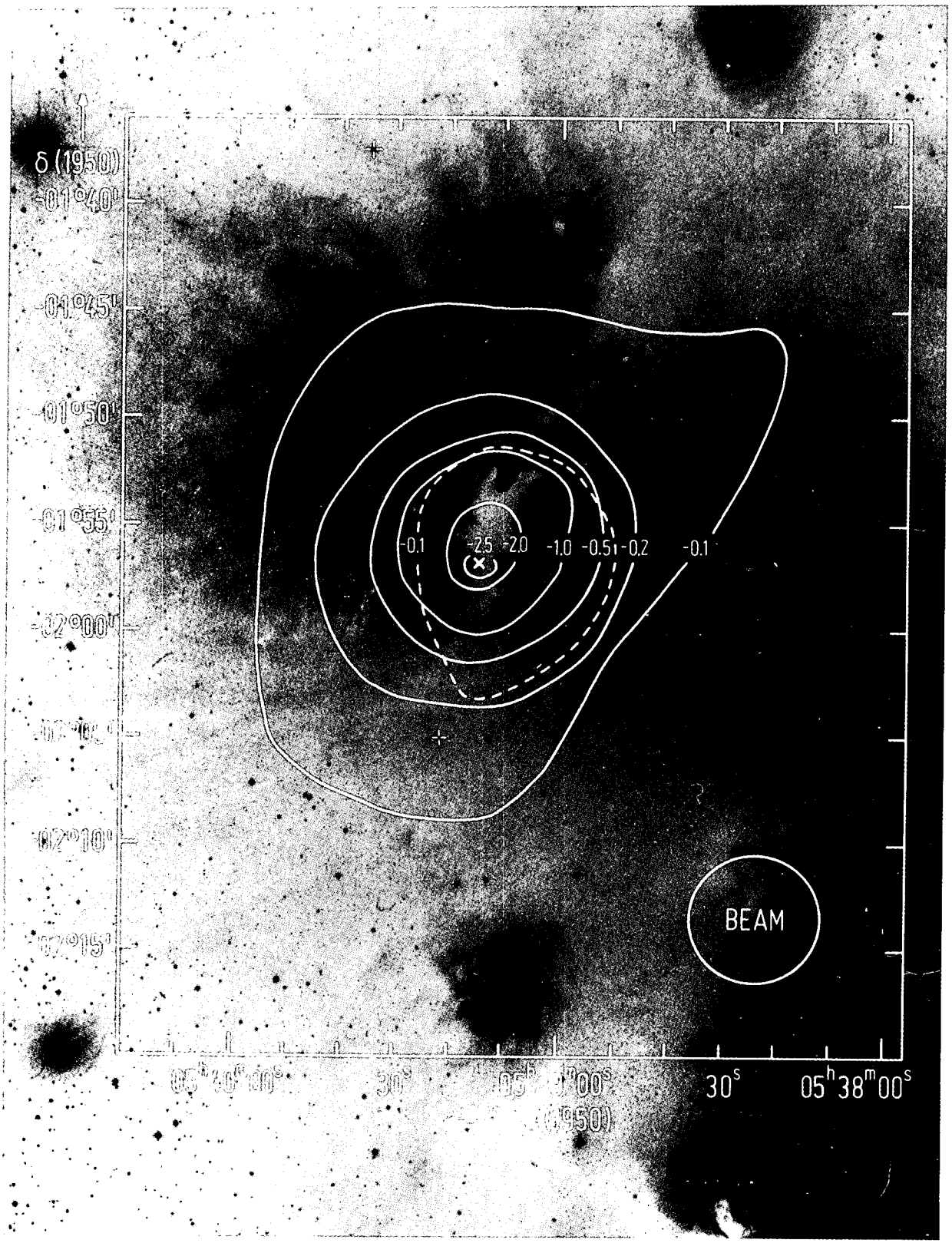

Fig. 1b. Contour map of the antenna temperature of the 19km s^{-1} H_2CO line in M17 superimposed on the Palomar Observatory Sky Survey red print. The unit of T_A is K. The radial velocities of the lines are shown in dashed lines.

The 19km s^{-1} cloud is extended toward the dark nebula in the northwest side covering the entire complex of the HII region and the dark cloud. This feature is also elongated along the north-south direction which is similar to the distribution of dark material. The intensity peak of this cloud also lies at the middle of the darkest part. The OH cloud at 17km s^{-1} observed by Gardner and McGee (1971) also has an intensity peak at the position of H_2CO peak. The bulge of the cloud in the southeastern corner as shown in Figure 1b is considered to be arising due to the contribution of the continuum emission from the HII region in the background.

The distribution of the equivalent width in this cloud is given in Figure 2. The equivalent width is calculated assuming that $T_{ex}=1.7K$ and that the molecular cloud is located in front of the continuum source. The equivalent width varies from 0.02 to 0.3km s^{-1}.

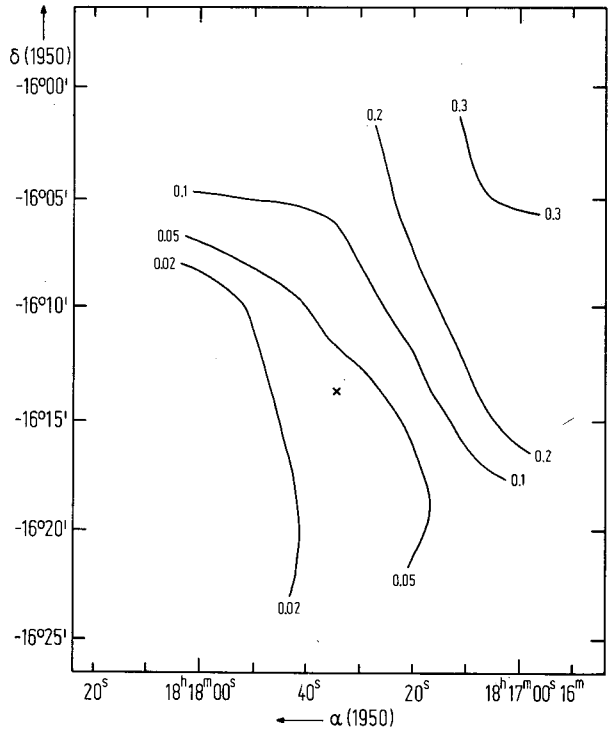

Fig. 2. Contour map of the equivalent width, $W=\int(1-e^{-\tau})\,dv$, of the 19km s^{-1} H_2CO line in M17. The unit is km s^{-1}.

The figure shows that the contour lines run parallel to the dark lane with the optical depth increasing toward the northwest direction. Other observations by Lada and Chaisson (1975) and Bieging *et al.* (1987) also show a similar distribution of optical depth. The northwestern edge of the dark lane has the maximum value of the equivalent width. Beyond this edge where there is a bright HII region, no H_2CO line was detected. It is clear that the 19km s^{-1} feature originates from the visible dark cloud located in front of the HII region at the northwest of the radio continuum source. In contrary, however, Lada (1976) stated in his CO survey paper that the HII region is located in front of the 20km s^{-1} CO cloud.

The angular size of the 19km s^{-1} cloud is about $20'\times15'$ in arc. The mean column density and mass of this cloud under the same assumptions as the 24km s^{-1} cloud are derived to be $N(H_2CO)=4.2\times10^{12}cm^{-2}$ and $M(H_2CO)=8\times10^{-5}M_\odot$ respectively. The total mass of the cloud is $M_{total}=1334M_\odot$, which is about 4 times of that of the 24km s^{-1} cloud.

2. Distribution in the Velocity-Position Plane

Figure 3a and 3b are the contour maps of the H_2CO line temperature in the velocity-position plane. Figure

3a is a plot along right ascension (east-west) at $\alpha\,(1950) = 18^h17^m40^s$ and 3b is a plot along declination (north -south) at $\delta\,(1950) = -16°15'$. The two clouds are blended together with a common outer envelope in the velocity range between 16 and 26km s^{-1}. The 24km s^{-1} feature is intense and smooth with a low velocity dispersion, while the 19km s^{-1} feature shows a considerable structure with two peaks in the $V_{LSR} - \Delta\alpha$ diagram and with a large velocity dispersion. The intensity peaks at 18.5km s^{-1} shown in both diagrams lie at ~ 3 arcmin west and ~ 11 arcmin north of the 24km s^{-1} cloud center, which coincides with the darkest part in the dust lane along the declination strip.

If the distribution along the radial velocity axis indicates the line-of-sight distribution as expected, the 19km s^{-1} cloud might be closer to us than the 24km s^{-1} as shown in the figure. There is almost no velocity gradient along either right ascension or declination axes. However, as can be seen in the both pictures, a small peak with the velocity of 18km s^{-1} is shown at the position, $\alpha\,(1950) = 18^h17^m29^s$, $\delta\,(1950) = -16°02'30''$ which coincides with the center of the dark lane. The 19km s^{-1} cloud in the direction of the 24km s^{-1} cloud center appears to be shifted to a higher velocity (21km s^{-1}) with a large line halfwidth (4km s^{-1}) as seen in Figure 3b. This seems to be an indication that the cloud is approaching toward the HII region.

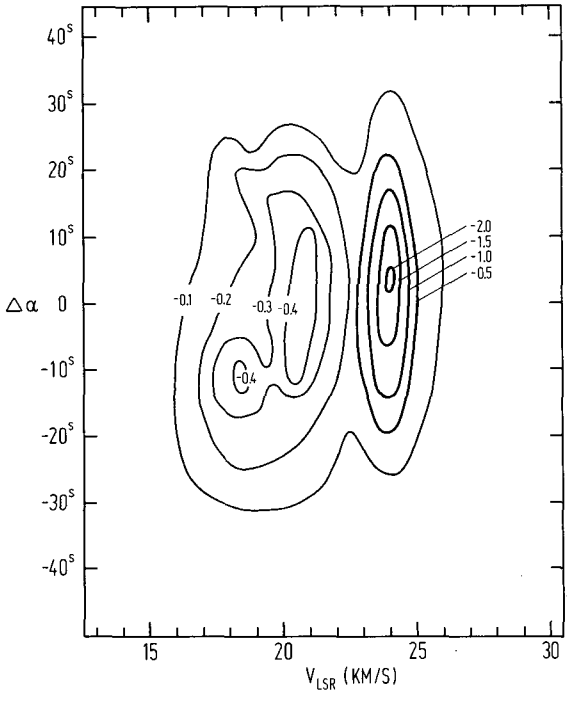

Fig. 3a. Contour map of the antenna temperature of the 24km s^{-1} H_2CO line in M17 in a space-velocity plane along $\delta_{1950} = -16°15'$. The ordinate shows the displacement from $\alpha_{1950} = 18^h17^m40^s$.

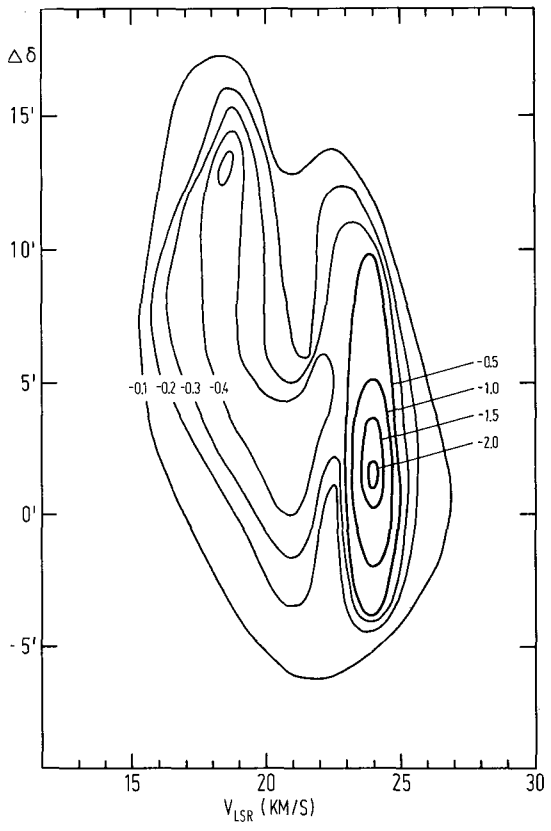

Fig. 3b. Contour map of the antenna temperature of the 19km s^{-1} H_2CO line in M17 in a space-velocity plane along $\alpha_{1950} = 18^h17^m40^s$. The ordinate shows the displacement from $\delta_{1950} = -16°15'$.

3. Radial Velocity Distribution

The velocity distribution shown in Figure 1a indicates that the 24km s^{-1} cloud has a small velocity gradient throughout the entire cloud in the direction to the north. The gradient is at a rate of $dv/d\delta = 0.1$km s^{-1} per

arcmin. This suggests either the cloud is rotating about an axis parallel to the right ascension or expanding or contracting along the direction of the velocity gradient. As already discussed by Lada and Chaisson (1975), if this is an indication of the cloud rotation, the rotational period is about 10^8 years.

We cannot determine in the present analysis the possibility of cloud contraction toward the cloud center which might be located somewhere near the northern edge of the cloud beyond which the H_2CO molecule is not detectable due to the reduced continuum background and small optical depth. The extended CO cloud also shows that there occurs a gradual velocity gradient throughout the entire cloud, increasing from 20km s^{-1} in the northeast to about 22km s^{-1} to the southwest (Elmegreen and Lada, 1976).

The velocity distribution of the 19km s^{-1} cloud is given in Figure 1b. It appears that there also presents a systematic velocity change increasing toward the southwest direction. The magnitude of the gradient is $\sim$0.4km s^{-1} per arcmin which is 4 times that of the 24km s^{-1} cloud. The gradient becomes steeper at the southern part of the cloud where the velocity is 20.5km s^{-1} at the edge. Our equi-velocity lines run parellel to the long axis of the dark lane at the low velocity but perpendicular to it at the high velocity. The CO observations (Lada, 1976; Elmegreen and Lada, 1976) also show a gradual velocity gradient which runs throughout the entire CO cloud from 20km s^{-1} in the northeast to about 22km s^{-1} far to the southwest which agrees well with the velocity gradient of the H_2CO cloud.

The linewidth of the 19km s^{-1} is generally uniform except the direction of the continuum peak where the 24km s^{-1} cloud center is located. Even in this direction the linewidth is shown to be much smaller than they estimated. This can be seen in Figure 3b where the line intensity is plotted in the δ-ΔV plane. We don't see any direct evidence of collape of the cloud. Lada (1976) also obtained a similar conclusion from his CO observations.

The overall picture of the distributions of HII region, molecular clouds, dust clouds in this region can be summerized as follows: The 24km s^{-1} cloud is part of the dimensionally much larger molecular cloud than what we detected in the vicinity of the HII region. This cloud might have a larger dimension than that of the radio source outside of which it is not detectable due to the low column density and weak microwave background which is non other than the 2.7K universal background. This cloud is moving toward the HII region with the radio recombination line velocity. Whether this part of collapsing motion or part of rotational motion is uncertain in this investigation. The 19km s^{-1} cloud is associated with the visible dark lane in front the HII region. This cloud is moving toward the HII region with a relative velocity of about 2km s^{-1}.

4. Radial Velocity Comparison with Other Radio Lines

All the available radial velocity data of molecular lines observed in the continuum peak positions and M17SW have been assembled in Table 1. Since the H_2O maser lines are highly variable, they are excluded.

The velocities of molecular lines in the direction of M17 range from 11 to 24km s^{-1}. But they can be divided into three groups; 11$\sim$12, 18$\sim$21, and 23$\sim$24km s^{-1}. Only OH, CH, and H_2CO lines observed by several authors (e.g. Gardner and McGee, 1971; Rydbeck *et al.*, 1974; Downes *et al.*, 1980; Bieging *et al.* 1987) have a component at 11km s^{-1}. This component, however, is extremely weak making them hardly distinguishable from the noise in many cases.

Most of the molecules observed in the directions of M17 and M17SW have components at 18$\sim$21km s^{-1} which is the same velocity of the H_2CO line observed mostly in the directions of dark clouds. The CO cloud is also closely associated with the dust lane west of the HII region with a similar velocity (Lata, 1976). The radio recombination lines (Goudis, 1975) have systematically lower velocities at $\sim$17km s^{-1} than those of molecular lines as already noted by Liszt (1973) who suggests a geometrical effect such as that a visible HII region is strongly ionization bounded when it meets the dense molecular cloud and will expand in the direction toward us. The H_2CO and OH lines which are observed in absorption have components at the velocity 24km s^{-1}. This is another indication that this cloud is physically associated with the continuum source behind the apparent dark lane.

Table 1. Molecular Lines and Their Velocities Observed in M17

Molecular line	Position (α_{1950}, δ_{1950})	V_{LSR} (km s^{-1})	Reference
OH (1667MHz abs.)	RS1	19.6	Goss (1968)
OH (1667MHz abs.)	$18^h17^m40^s$, $-16°12.6'$	11.5	Gardner & McGee (1971)
		19.5	
		23	
OH ($^2\Pi_{3/2}$, J=5/2, F=3-3)	$18^h17^m31.9^s$, $-16°12'48''$	21.0	Knowles *et al.* (1976)
		22.1	
CO (J=1-0)	RS1	21	Schwartz *et al.* (1973)
CO (J=1-0)	RS1	21	Wilson *et al.* (1974)
CO (J=1-0)	SW	18	Lada *et al.* (1974)
CO (J=1-0)	SW	20.2	Lada (1976)
CO (J=1-0)	$18^h17^m26.5^s$, $-16°14'54''$	20	Goldsmith *et al.* (1975)
CO (J=2-1)	SW	21	Cronin *et al.* (1976)
CO (J=2-1)	$18^h17^m26.5^s$, $-16°14'54''$	20	Goldsmith *et al.* (1975)
CO (J=4-3)	SW	20.3	Schulz & Krugel (1987)
^{13}CO (J=1-0)	SW	18	Lada *et al.* (1974)
^{13}CO (J=1-0)	RS1	20	Wilson *et al.* (1974)
^{13}CO (J=1-0)	SW	20.2	Lada (1976)
$C^{18}O$ (J=1-0)	SW	18	Lada *et al.* (1974)
$C^{18}O$ (J=1-0)	SW	19.9	Lada (1976)
$C^{18}O$ (J=2-1)	SW	19	Stutzki & Gusten (1990)
H_2CO (1_{11}-1_{10})	$18^h17^m36^s$, $-16°12'17''$	23.2	Zuckerman *et al.* (1970)
H_2CO (1_{11}-1_{10})	$18^h17^m33.6^s$, $-16°13'23''$	11.6	Downes *et al.* (1980)
		23.5	
H_2CO (1_{11}-1_{10})	RS1	22.8	Whiteoak & Gardner (1970)
H_2CO (1_{11}-1_{10})	RS2	11.1	Whiteoak & Gardner (1970)
		22.7	
H_2CO (1_{11}-1_{10})	SW	18.9	Lada & Chaisson (1975)
		24.0	
H_2CO (1_{11}-1_{10})	$18^h17^m36^s$, $-16°12'17''$	23.4	Matsakis *et al.* (1976)
H_2CO (1_{11}-1_{10})	$18^h17^m33^s$, $-16°12'47''$	11	Bieging *et al.* (1982)
		18	
		24	
H_2CO (2_{11}-1_{11})	SW	19.7	Mundy *et al.* (1987)
H_2CO (2_{11}-2_{10})	SW	19.0	Mundy *et al.* (1987)
H_2CO (2_{11}-2_{12})	RS1	12.1	Gardner & Whiteoak (1984)
		20.1	
		24.0	
H_2CO (2_{11}-2_{12})	SW	18	Lada *et al.* (1974)
H_2CO (2_{11}-2_{12})	SW	20.4	Lada (1976)
H_2CO (2_{11}-2_{12})	SW	20.6	Mundy *et al.* (1987)
H_2CO (2_{12}-1_{11})	SW	19.75	Lada (1976)
H_2CO (3_{13}-2_{12})	SW	19.3	Mundy *et al.* (1987)
H_2CO (3_{12}-2_{11})	SW	19.3	Mundy *et al.* (1987)
H_2CO (4_{14}-3_{13})	SW	19.9	Mundy *et al.* (1987)
HCN (J=1-0)	SW	20	Baudry *et al.* (1980)
HCN (J=1-0)	RS1	23	Wilson *et al.* (1974)
HCN (J=1-0)	SW	18	Lada *et al.* (1974)
HCN (J=1-0)	SW	19.5	Gottlieb *et al.* (1975)
CS (J=1-0)	SW	19.7	Lada (1976)
^{13}CS (J=1-0)	SW	18.4	Lada (1976)
$C^{34}S$ (J=1-0)	SW	19	Lada (1976), Stutzki & Gusten (1990)
CS (J=3-2)	SW	20.0	Lada (1976), Greaves *et al.* (1992)

Table 1. Continued.

CH	SW	12	Rydbeck *et al.* (1974)
		24	
C_2H (N=1-0)	SW	19.5	Tucker *et al.* (1974)
HCO^+ (J=1-0)	$18^h17^m26.5^s$, $-16°14'54''$	20	Baudry *et al.* (1980)
NH_3 (1, 1, ΔF=1)	$18^h17^m10^s$, $-16°12.0'$	20	Schwartz *et al.* (1977)
NH_3 (1, 1, F=1-0)	SW	18.9	Lada (1976)
NH_3 (1, 1, F=1-2)	SW	19.4	Lada (1976)
NH_3 (1, 1, F=2-2)	SW	19.2	Lada (1976)
NH_3 (1, 1, F=2-1)	SW	19.7	Lada (1976)
NH_3 (1, 1, F=0-1)	SW	19.3	Lada (1976)
NH_3 (2, 2)	SW	20.8	Lada (1976)
SO ($J_K=4_3-3_2$)	SW	18	Lada *et al.* (1974)

RS1: Radio source 1 ($\alpha_{1950}=18^h17^m34.7^s$, $\delta_{1950}=-16°13'48''$)
RS2: Radio source 2 ($\alpha_{1950}=18^h17^m36.7^s$, $\delta_{1950}=-16°10'43''$)
SW: Southwest source ($\alpha_{1950}=18^h17^m26.5^s$, $\delta_{1950}=-16°14'54''$)

IV. FORMALDEHYDE IN NGC 2024

1. Intensity Distribution

There are detected two H_2CO lines in the directions of dark clouds in NGC 2024; one, an intense feature at $\sim$9km s^{-1} which is extended along the dark bar, and the other, a weak probable feature at $\sim$13km s^{-1} confined to the immediate vicinity of the radio continuum. In Figure 4, the contour lines of the H_2CO line temperature of both 9 and 13km s^{-1} features are shown on the POSS print. The maximum temperature of the 13km s^{-1} H_2CO line is ~ -0.14K. Both clouds have concentric circular contours with the center coinciding with the radio continuum source and the dark lane. The H_2CO distribution is very similar to that of the radio continuum measured in the nebula (Schraml and Mezger, 1969; Gordon, 1969). The position of the H_2CO line intensity peak coincides with the peaks of radio continuum and other molecular distribution [e.g. NH_3 and CS (Schulz *et al.*, 1991)].

The radio H recombination line survey of the nebula also shows a single source with lines of the Gaussian shape (Gordon, 1969). The radio continuum is only detected at the region within the contour of H_2CO temperature -0.2K. The lowest contour line of -0.1K has an elliptical shape whose major axis is parallel to the dark bar and an extended wing to the northwest direction where a dark cloud is present. The cold HI observed in absorption is also extended into the northwest direction (Lockhart and Goss, 1978). The distribution maps of CS and HCN show a similar elongation in the north-south direction (Thronson *et al.*, 1984).

The distribution of the linewidth is nearly uniform at $\sim$1.7km s^{-1}. The absence of any systematic change of the linewidth toward the cloud center suggests that there is no systematic mass motion of the gas in the cloud. The distribution of the equivalent width is given in Figure 5. The maximum equivalent width in this cloud is $\sim$0.5km s^{-1}. The general shape of the equivalent width distribution is similar to the distribution of the line temeprature with coinciding centers, near circular central contours, and elongations into the northwest and the southeast directions. It is clear that the 9km s^{-1} feature is associated with the visual dark lane located in front of the HII region or the radio continuum source. Thronson *et al.* (1984) also reached the same conclusion from their CS and HCN observations.

The angular size of this cloud is about $20'\times15'$ in arc which corresponds to 6.4pc^2 at a distance 0.5kpc. The mean column density and mass of the H_2CO cloud are N (H_2CO) $=1.1\times10^{13}$cm^{-2} and M (H_2CO) $=1.75\times10^{-5}M_\odot$ respectively. The total mass of the cloud is $M_{total}=350M_\odot$.

The 13km s^{-1} feature is detected only in the central region of the dark lane which happens to coincide with the radio continuum source direction. The line temperature of this feature is not showing the effect of the continuum source maintaining a constant value at $\sim$0.14K. This temperature is about the same as the line temperature of the region of periphery of the 9km s^{-1} cloud. Thus, it is highly probable that this feature arises from a cloud behind the radio source.

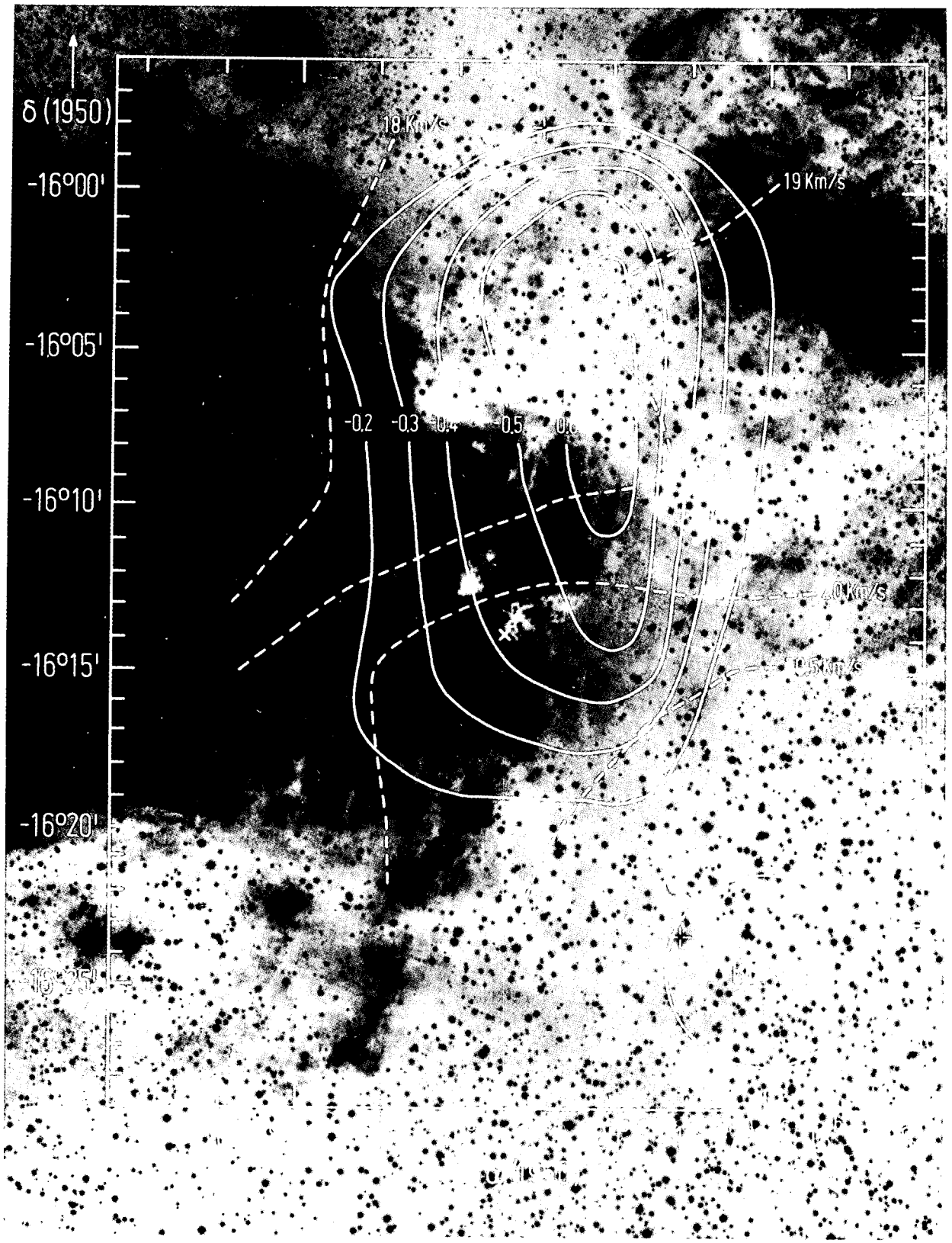

Fig. 4. The antenna temperature distribution of the 9km s^{-1} (solid line) and the 13km s^{-1} (dashed line) lines in NGC 2024 superimposed on the Palomar Observatory Sky Survey red print. The unit is K.

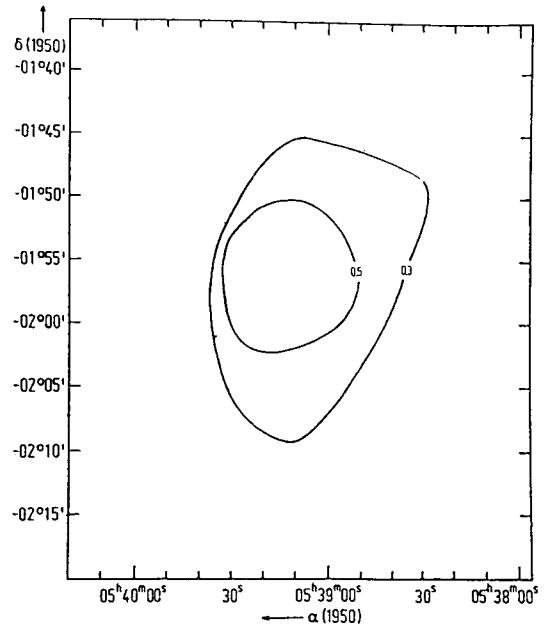

Fig. 5. The distribution of the equivalent width of the 9km s^{-1} line in NGC 2024. The unit is km s^{-1}.

2. Kinematics

The radial velocity distribution of the 9km s^{-1} feature is given in Figure 6. The velocity varies from 9.5 to 12.0km s^{-1}. The central part of this cloud has the lowest velocity, while the northern and southern parts have

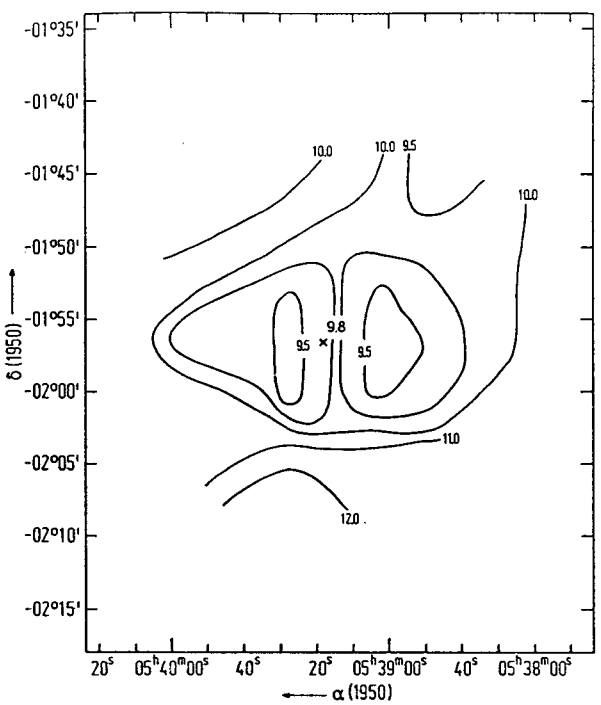

Fig. 6. The radial velocity distribution of the 9km s^{-1} line in NGC 2024. The unit is km s^{-1}.

higher velocities. Watt *et al.* (1979) observed a small velocity gradient across the southern CO hotspot increasing from the northwest to the southeast directions in ^{13}CO and ^{12}CO mappings. The velocities of the HI absorption lines (Lockhard and Goss, 1978), H and C 134α lines (Wilson *et al.*, 1975), and H 94α recombination line increase with a similar orientation by more than 3km s^{-1}.

V. RADIAL VELOCITY COMPARISON WITH OTHER MOLECULAR LINES

All the molecular line velocities observed at NGC 2024 are tabulated in Table 2. Molecular lines show that

Table 2. Molecular Lines and Their Velocities Observed in NGC 2024

Molecular line	Position (α_{1950}, δ_{1950})	V (km s^{-1})	Reference
OH (1612MHz)	RS	9.3~12.7	Goss *et al.* (1976)
OH (1665MHz)	RS	9.3	Goss *et al.* (1976)
		11.2	
OH (1667MHz)	RS	9.5	Goss *et al.* (1976)
		11.4	
		12.7	
OH (1720MHz)	RS	9.3	Goss *et al.* (1976)
		10.7	
OH (1612, 1665, 1667, 1720)	RS	9.5	Goss *et al.* (1976)
CO (J=1-0)	RS	9.6	Tucker *et al.* (1973)
CO (J=1-0)	$05^h39^m13^s$, $-01°55'48''$	11	Wilson *et al.* (1974)
CO (J=1-0)	$05^h39^m07^s$, $-01°55'42''$	9.6	Milman *et al.* (1975)
CO (J=1-0)	RS	11	Goldsmith *et al.* (1975)
CO (J=2-1)	RS	9	Goldsmith *et al.* (1975)
^{13}CO (J=1-0)	RS	9.8	Tucker *et al.* (1973)
^{13}CO (J=1-0)	RS	11	Goldsmith *et al.* (1975)
^{13}CO (J=2-0)	RS	10	Goldsmith *et al.* (1975)
H_2CO (1_{10}-1_{11})	RS	8.6	Zuckerman *et al.* (1970)
H_2CO (1_{10}-1_{11})	RS	9.4	Matsakis *et al.* (1976)
		11.5	
H_2CO (1_{10}-1_{11})	RS	9.4	Wilson (1972)
H_2CO (1_{10}-1_{11})	RS	8.6	Whiteoak & Gardner (1970)
		12.4	
		24.8	
H_2CO (1_{10}-1_{11})	$05^h39^m15^s$, $-01°55'42''$	9.3	Bieging *et al.* (1982)
		12.8	
H_2CO (2_{11}-2_{12})	RS	9.3	Henkel *et al.* (1980)
H_2CO (2_{11}-1_{11})	$05^h39^m13^s$, $-01°56'58''$	10.8	Mundy *et al.* (1987)
H_2CO (2_{11}-1_{11})	$05^h39^m13^s$, $-01°56'58''$	10.9	Mundy *et al.* (1987)
H_2CO (3_{13}-2_{11})	$05^h39^m13^s$, $-01°56'58''$	11.1	Mundy *et al.* (1987)
H_2CO (4_{14}-3_{13})	$05^h39^m13^s$, $-01°56'58''$	11.0	Mundy *et al.* (1987)
H_2CO (3_{12}-2_{11})	$05^h39^m13^s$, $-01°56'58''$	11.0	Mundy *et al.* (1987)
$H_2{}^{13}CO$ (1_{10}-1_{11})	RS	8.6	Zuckerman *et al.* (1969)
$H_2{}^{13}CO$ (1_{10}-1_{11})	$05^h39^m14^s$, $-01°56'12''$	9.2	Henkel *et al.* (1982)
HCO ($N_{KK}=1_{01}$-0_{00})	$05^h39^m14^s$, $-01°56'12''$	9.8	Snyder *et al.* (1976)
HCN (J=1-0)	$05^h39^m13.5^s$, $-01°56'57''$	11.2	Morris *et al.* (1974)
CS (J=1-0)	$05^h39^m13.5^s$, $-01°56'57''$	11.0	Morris *et al.* (1974)
SO (3_2-2_1)	RS	9.8	Gottlieb & Ball (1973)
SO (4_3-3_2)	RS	10.1	Gottlieb & Ball (1973)
NH_3 (1, 1, $\Delta F=1$)	$05^h39^m12^s$, $-01°55'48''$	9	Schwartz *et al.* (1977)

RS: Radio source position ($\alpha_{1950}=05^h39^m12^s$, $\delta_{1950}=-01°55'42''$)

there are two clouds at velocity ranges of 8~10 and 11~13km s^{-1}. Whiteoak and Gardner (1970) lists an additional H_2CO line at 24km s^{-1} which is not shown in this study. The radial velocities of various radio recombination lines are in the range between 8.2 and 10km s^{-1}, which is in good agreement with the 9km s^{-1} H_2CO line velocity. The radial velocity of the HI absorption line also has a similar value of 10.4km s^{-1} (Lockhart and Goss, 1978). A similar velocity gradient from the northwest to the southwest directions is apparent in the HI absorption line and the H94α recombination line which are mapped by Lockhart and Goss (1978) and Gordon (1969) respectively. But the magnitude of the gradient is 2 to 3 times less for the HI absorption line.

VI. SUMMARY

We have mapped the dark clouds in M17 and NGC 2024 in the 6-cm H_2CO absorption line. In M17, we detected two H_2CO clouds with velocities of 19km s^{-1} and 24km s^{-1}. The 19km s^{-1} cloud which has a larger extent and is located in front of the 24km s^{-1} cloud appears to be associated with the visual dark dust lane in the region. The equivalent width increase toward the northwest direction. The angular size and total mass of this cloud are about $20' \times 15'$ in arc and $1335 M_\odot$ respectively.

The 24km s^{-1} cloud is located at the immediate vicinity of the radio continuum source. This line arises by the absorption of the radio continuum from the HII region behind the dark lane. The mean optical depth is generally uniform throughout the cloud. But the equivalent width increases toward the north. This cloud is elongated along the north-south direction which is similar to the shape of the dark lane. The angular size and total mass of this cloud are about $14' \times 11'$ in arc and $330 M_\odot$ respectively.

The above two clouds in M17 are physically connected in the direction of the line of sight with a common envelope. The 19km s^{-1} cloud in the vicinity of the 24km s^{-1} appears to be approaching toward the HII region.

In both clouds in M17, a velocity gradient from the northease to the southwest directions is observed. The linewidths are uniform throughout the clouds. The radial velocities of various molecular lines are generally in agreement.

In NGC 2024, there are detected two line components at 9km s^{-1} and 13km s^{-1}. The 9km s^{-1} cloud appears to be physically associated with the dark bar in front the HII region and the radio source. The 13km s^{-1} feature is probably arising by the absorption of the microwave background radiation by a cloud associated with the HII region but located at the immediate behind the radio source. Many other molecules also have lines at the similar velocities as those of H_2CO lines.

REFERENCES

Altenhoff, W. J., Downes, D., Pauls, T. & Schraml, J. 1979, A&AS, 35, 23
Baudry, A., Combes, A., Perault, M. & Dickman, R. 1980, A&A, 85, 244
Bieging, J. H., Wilson, T. L. & Downes, D. 1982, A&AS, 49, 607
Chini, R., Elsässer, H. & Neckel, Th. 1980, A&A, 91, 186
Cronin, N. J., Gillespie, A. R., Huggins, P. J. & Phillips, T. G. 1976, A&A, 46, 135
Downes, D., Wilson, T. L., Bieging, J. & Wink, L. 1980, A&AS, 40, 379
Elmegreen, B. G. & Lada, C. J. 1976, AJ, 81, 1089
Gardner, F. & McGee, R. X. 1971, ApJ, 8, L83
Gardner, F. & Whiteoak, J. B. 1984, MNRAS, 210, 23
Goldsmith, P. F., Plambeck, R. L. & Chiao, R. Y. 1975, ApJ, 196, L39
Gordon, M. A. 1969, ApJ, 158, 479
Goss, W. M. 1968, ApJS, 15, 131
Goss, W. M., Winnberg, A., Johansson, L.E.B. & Fournier, A. 1976, A&A, 46, 1
Gordon, M. A. 1969, ApJ, 158, 479
Gottlieb, C. A. & Ball, J. A. 1973, ApJ, 184, L59
Gottlieb, C. A., Lada, C. J., Gottlieb, E. W., Lilley, A. E. & Litvak, M. M. 1975, ApJ, 202, 655

Goudis, C. 1975, ApSS, 38, 13
Goudis, C. 1976, ApSS, 39, 273
Greaves, J. S., White, J. & Williams, P. G. 1992, A&A, 257, 731
Henkel, C., Walmsley, C. M. & Wilson, T. L. 1980, A&A, 82, 41
Henkel, C., Wilson, T. L. & Bieging, J. 1982, A&A, 109, 344
Knowles, S. H., Caswell, J. L. & Goss, W. M. 1976, MNRAS, 175, 537
Lada, C., Dickinson, D. F. & Penfield, H. 1974, ApJ, 189, L35
Lada, C. & Chaisson, E. J. 1975, ApJ, 195, 367
Lada, C. 1976, ApJS, 32, 603
Liszt, H. S. 1973, Ph.D. Thesis, Princeton University
Lockart, A. & Goss, W. M. 1978, A&A, 67, 355
Matsakis, D. N., Chui, M. F. & Goldsmith, P. F. & Townes, C. H. 1976, ApJ, 206, L63
Massi, M., Churchwell, E. & Felli, M. 1988, A&A, 194, 116
Mezger, P. G. & Henderson, A. P. 1967, ApJ, 147, 471
Milman, A. S., Knapp, G.R., Kerr, F. G., Knapp, S. L. & Wilson, W. J. 1975, AJ, 80, 93
Minn, Y. K. & Greenberg, J. M. 1979, A&A, 77, 37
Morris, M., Palmer, P., Turner, B. E. & Zuckermann, B. 1974, ApJ, 191, 349
Mundy, S. G., Evans II, N. J., Snell, R. L. & Goldsmith, P. F. 1987, ApJ, 318, 392
Rainey, R., White, G. J., Gatley, I., Hayashi, S. S., Kaifu, N., Griffin, M. J., Monteiro, T. S., Cronin, N. J. & Scivetti, A. 1987, A&A, 171, 252
Rydbeck, O.E.H., Ellder, J., Irvine, W. M., Sume, A. & Hjalmarson, A. 1974, A&A, 33, 315
Schraml, J. & Mezger, P. G. 1969, ApJ, 156, 269
Schulz, A. & Krugel, E. 1987, A&A, 171, 297
Schwartz, P. R., Willson, W. J. & Epstein, E. E. 1973, ApJ, 186, 529
Schwartz, P. R., Cheung, A. C., Bologna, J. M., Chui, M. F., Waak, J. A. & Matsakis, D. 1977, ApJ, 218, 671
Stutzki, J. & Gusten, R. 1990, ApJ, 356, 513
Thronson, H. A. & Lada, C. J. 1983, ApJ, 269, 175
Thronson, H. A., Lada, C. J., Schwartz, P. R., Smith, H. A., Smith, J., Glaccum, W., Harper, D. A. & Loewenstein, R. F. 1984, ApJ, 280, 154
Tucker, K., Kutner, M. & Thaddeus, P. 1973, ApJ, 186, L13
Tucker, K. D., Kutner, M. L. & Thaddeus, P. 1974, ApJ, 193, L115
Snyder, L. E., Hollis, J. M. & Ulich, B. L. 1976, ApJ, 208, L91
Watt, G. D., White, G. J., Cronin, N. J. & van Vliet, A.H.F. 1979, MNRAS, 189, 287
Whiteoak, J. B. & Gardner, F. F., 1970, ApL, 5, 5
Wilson, T. L. 1972, A&A, 19, 354
Wilson, W. J., Schwartz, P. R., Epstein, E. E., Johnson, W. A., Etcheverry, R. D., Mori, T. T., Berry, G. G. & Dyson, H. B. 1974, ApJ, 191, 357
Wilson, T. L., Thomasson, P. & Gardner, F. F. 1975, A&A, 43, 167
Zuckerman, B., Palmer, P., Snyder, L. E. & Buhl, D. 1969, ApJ, 157, L167
Zuckerman, B., Buhl, D., Palmer, P. & Snyder, L. E. 1970, ApJ, 160, 485